

TianQuan-Climate: A Subseasonal-to-Seasonal Global Weather Model via Incorporate Climatology State

Guowen Li¹, Xintong Liu¹, Shilei Cao¹, Haoyuan Liang¹, Mengxuan Chen², Lixian Zhang³, Jinxiao Zhang², Jiuke Wang¹, Meng Jin⁴, Juepeng Zheng^{1*} and Haohuan Fu²

¹Sun Yat-sen University

²Tsinghua University

³National Supercomputing Center in Shenzhen

⁴Huawei Technologies Co., Ltd

{ligw8, liuxt69, caoshlei, lianghy68}@mail2.sysu.edu.cn, {chenmx21, zhang-jx22}@mails.tsinghua.edu.cn, zhanglx18@tsinghua.org.cn, jinmeng13@huawei.com, zhengjp8@mail.sysu.edu.cn, haohuan@tsinghua.edu.cn

Abstract

Subseasonal forecasting serves as an important support for Sustainable Development Goals (SDGs), such as climate challenges, agricultural yield and sustainable energy production. However, subseasonal forecasting is a complex task in meteorology due to dissipating initial conditions and delayed external forces. Although AI models are increasingly pushing the boundaries of this forecasting limit, they face two major challenges: **error accumulation** and **Smoothness**. To address these two challenges, we propose Climate Furnace Subseasonal-to-Seasonal (TianQuan-Climate), a novel machine learning model designed to provide global daily mean forecasts up to 45 days, covering five upper-air atmospheric variables at 13 pressure levels and two surface variables. Our proposed TianQuan-Climate has two advantages: 1) it utilizes a multi-model prediction strategy to reduce system error impacts in long-term subseasonal forecasts; 2) it incorporates a Content Fusion Module for climatological integration and extends ViT with uncertainty blocks (UD-ViT) to improve generalization by learning from uncertainty. We demonstrate the effectiveness of TianQuan-Climate on benchmarks for weather forecasting and climate projections within the 15 to 45-day range, where TianQuan-Climate outperforms existing numerical and AI methods.

1 Introduction

Subseasonal forecasting is crucial for Sustainable Development Goals (SDGs), including sustainable energy, climate change challenge and water management [Pegion *et al.*, 2019]. Over the past 40 years, Numerical Weather Prediction (NWP) models have significantly advanced weather forecasting skills for the short to medium term, contributing no-

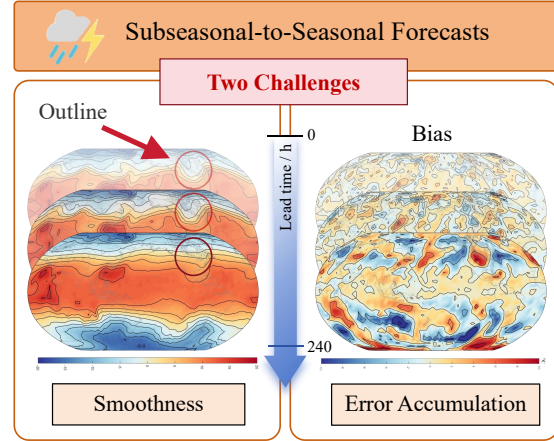


Figure 1: **Two Major Challenges in Subseasonal-to-Seasonal (S2S) Forecasts.** As the forecast lead time extends, the results tend to become smoother, causing the outlines to gradually disappear (left) and the bias increase, leading to cumulative errors (right).

table to SDGs, particularly in energy management and climate decision-making responses [Bauer *et al.*, 2015]. While NWP methods offer accurate and stable predictions, they require substantial computational resources and time [Saha *et al.*, 2014]. Even with supercomputers operating on hundreds of nodes, simulating a single variable can take hours [Bauer *et al.*, 2020]. Moreover, the parameterization within NWP models introduces errors due to function approximations [Bellaars *et al.*, 2018]. In contrast, emerging machine learning (ML) models present a promising future due to their comparable accuracy and much faster inference speeds [Cohen *et al.*, 2019]. Once trained, these models can predict future weather conditions in seconds, highlighting their distinct advantages [Pathak *et al.*, 2022].

Recent developments [Bi *et al.*, 2023; Lam *et al.*, 2023; Chen *et al.*, 2023; Price *et al.*, 2024] in short and medium-term weather forecasting indicate that ML-based models can surpass NWP methods. While subseasonal forecast-

*Corresponding author

ing (forecasts beyond 15 days) is still treated as a "predictability desert", it is particularly essential for the prevention of extreme weather disasters [Vitart *et al.*, 2019; Robertson *et al.*, 2020] and renewable energy integration. The extended time horizon renders the weather initial conditions and key variables at hand inadequate for making accurate predictions [Mariotti *et al.*, 2018] due to the chaotic nature of the weather system. Nevertheless, ML-based approaches still face significant limitations in subseasonal forecasting. Deterministic machine learning models typically use training data that only includes data from nearby time periods, which is insufficient to support an effective learning process for subseasonal forecasting [He *et al.*, 2019]. The longer the forecast horizon, the less relevant the initial state becomes for weather predictions, leading to increasingly unrealistic and blurred predictions. This limitation makes it difficult for machine learning-based models to operate effectively on the subseasonal time scales required for climate modeling [Lam *et al.*, 2023; Bonavita, 2023].

Specifically, intricate patterns might fade in the subseasonal predictions of existing models and the bias of the actual observed values increases over time, as shown in Figure 1. In response to the above situation, we summarize the issues into two key points: **(1) Error accumulation.** Most autoregressive iterative forecasting methods suffer from significant error accumulation due to the inherent errors in the reanalysis data and the systematic biases of the model. **(2) Smoothness.** Since current methods rely on the initial state for subseasonal prediction, the low correlation between the initial state and the subseasonal prediction leads to overly smooth outputs.

To overcome these challenges, we propose TianQuan-Climate, where TianQuan (meaning Weather Hub in Chinese) reflects the model's role as a central forecasting system that integrates historical climate factors to assist subseasonal climate predictions. The model utilizes a multi-model forecasting strategy, as shown in Figure 2, to reduce the frequency of model system error impacts during long-term predictions. Additionally, two core components are proposed to optimize the model's single-step prediction results.

Specifically, we train models with different lead times (e.g., 15-45 days, with a trained model every 5-day interval) to perform subseasonal forecasting for up to 45 days, addressing the issue of error accumulation that occurs when a single lead-time model propagates its previous step's errors into subsequent predictions. To further enhance the model, we designed a Content Fusion Module to integrate trend features of the climatological mean state at the forecast time, mitigating the issue of missing information during the subseasonal forecasting process. Furthermore, our backbone innovatively extends the traditional Vision Transformer with uncertainty blocks (UD-ViT), allowing the injection of Gaussian noise as uncertainty term. The noise approximates the system model bias, and the backbone network improves the model's generalization by learning this uncertainty term.

In summary, our main contributions are as follows.

- We proposed a long-term forecasting framework named TianQuan-Climate with up to 45-day prediction, leveraging a multi-model approach to effectively mitigate error accumulation.

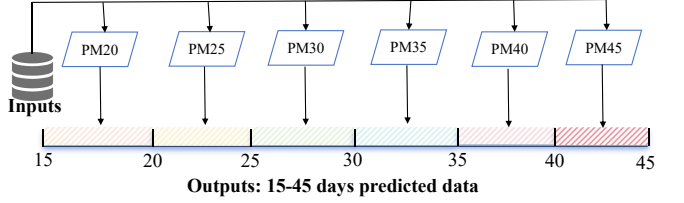


Figure 2: **Multi-model forecasting strategy.** $PM\mathcal{K}$ denotes forecast models with \mathcal{K} -day lead times. With at least 5 days of input data, predictions can be made for the following 15-45 days.

- We design the Content Fusion Module and the UD-ViT, which help to gain additional learnable climatological information, and yield more detailed and accurate prediction results, respectively.
- Our proposed TianQuan-Climate outperforms traditional models and AI methods (e.g., RMSE reduced by 21% vs. ECMWF-S2S, 10% vs. ClimaX) for subseasonal-to-seasonal forecasting, providing more detailed insights on subseasonal timescales.

2 Related Work

Machine Learning in weather forecasts. Weather forecasting primarily involves gridded prediction tasks, which can be viewed as image-to-image translation problems. In recent years, significant advancements have also been made in short- to medium-term weather and climate forecasting. Notable examples include FourCastNet [Pathak *et al.*, 2022], which was the first to attempt multi-variable forecasting in the short term with results comparable to NWP models. This was followed by the emergence of Pangu-Weather [Bi *et al.*, 2023] and GraphCast [Lam *et al.*, 2022], which surpassed traditional numerical methods in achieving multi-variable forecasting in the medium term. Researchers are now exploring ways to extend forecasting capabilities to even longer time scales [Kochkov *et al.*, 2024; Chen *et al.*, 2024]. However, at sub-seasonal to seasonal time scales, the predictive results of machine learning methods often lack of details about atmospheric states, leading to a significant reduction in forecast usability. To enhance the ability to predict the details of outline, we proposed the Content Fusion Module and extend the UD-ViT, which improve adaptability and accuracy in these long-term forecasting scenarios.

Subseasonal-to-Seasonal forecasts. Subseasonal forecasting, which provides predictions 2 to 6 weeks ahead, fills the crucial gap between short-term weather forecasts (typically up to 15 days) and long-term climate predictions that extend to seasonal and longer timescales [of Sciences *et al.*, 2016]. Although machine learning models have achieved significant progress in medium-range and climate prediction [Wang *et al.*, 2024], their effectiveness in subseasonal forecasting has been less pronounced [He *et al.*, 2021]. The primary limitation arises from the input data for the forecasting model, which only includes climate data at the forecast's initial time, insufficient to capture the critical variation information required for sub-seasonal to seasonal forecasts [Vitart *et al.*,

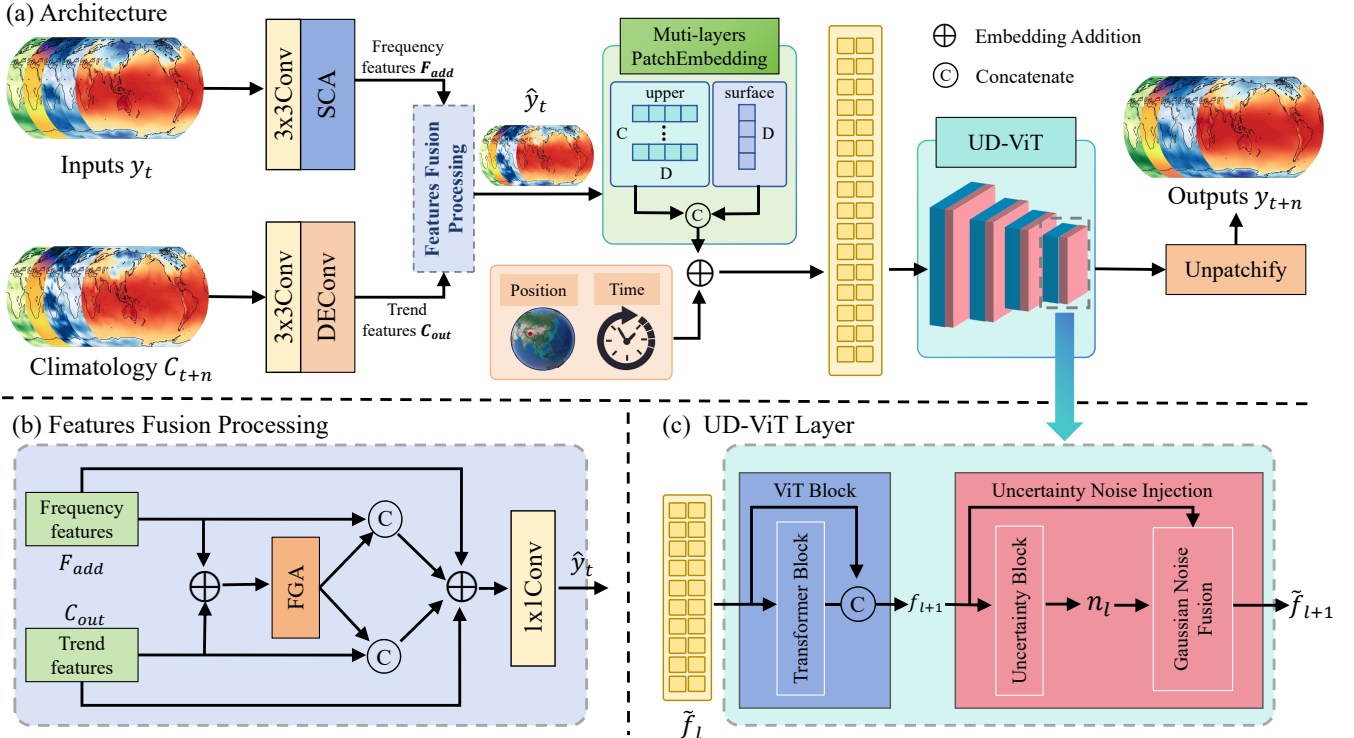


Figure 3: (a) **Model schematic diagram of the TianQuan-Climate**. The input variables include current daily average data y_t and climatological mean state C_{t+n} . After feature enhancement and fusion, they undergo patch embedding. The position and lead time embeddings are then fed into the UD-ViT backbone. (b) **Features Fusion Processing** enhances and fuses feature information. (c) **UD-ViT Layer** shows the detailed operation part of the neural network layer.

2022; Nathaniel *et al.*, 2024]. This limitation leads to iterative errors in long-term forecasts, ultimately rendering the results unusable [Lam *et al.*, 2023]. To address this, we introduce a multi-model forecasting strategy, which can effectively reduce the problem of system error accumulation.

3 Proposed Model

The proposed TianQuan-Climate model differs from autoregressive or roll-out methods by employing distinct models for each forecast range, as shown in Figure 2. For example, a 20-day model is used for the 15-20 day range, a 25-day model for the 21-25 day range, and so on up to 45 days. The modifications in the TianQuan-Climate model consist of two main components. **The first module** is the Content Fusion Module, which utilizes both daily average data and climate mean state data for forecasting. These inputs are separately processed using Spatial-Channel Attention (SCA) and Detail-enhanced Convolution (DECov), as illustrated in Figure 3(a). The trend features and high-frequency features extracted from the upper layers are then fused using Feature-guided Attention (FGA), as shown in Figure 3(b). This module ensures that long-term weather patterns are preserved. **The second module** is the Uncertainty block Vision Transformer (UD-ViT), as illustrated in Figure 3(c), which processes the features obtained through PatchEmbedding and learns the uncertainty noise's impact on the model's generalization. The model then applies Unpatchify to generate

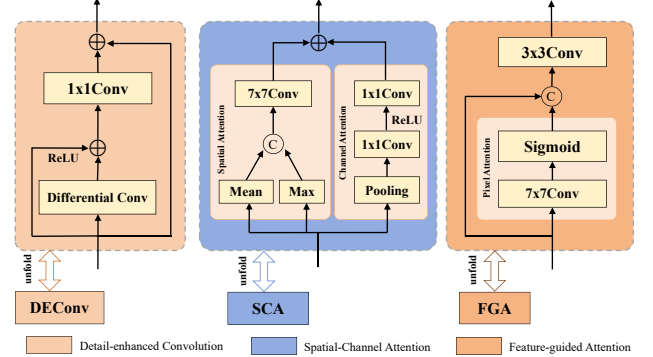


Figure 4: **The Three Components of the Content Fusion Module**. After extracting features using Detail-Enhanced Convolution (DEConv) and Spatial-Channel Attention (SCA), information is fused through Feature-Guided Attention (FGA).

ate spatio-temporal prediction results, resulting in more pronounced feature contours. The details of our proposed architecture are described below.

3.1 Input Representation

We perform the prediction task on grid-based data, where the inputs consists of daily average data t inputs y_t and the climatological mean state at the prediction time $t + n$ denoted as C_{t+n} . The climatological mean state is obtained by averaging val-

ues from the same time points over many years. Both of them are represented as $V \times H \times W$. Here, V denotes the number of variables, which may include surface and atmospheric state such as temperature and wind speed, or surface variables like 2-meter temperature. H and W represent the height and width of the variable grid, determined by the spatial resolution. In this work, we focus on spatial resolutions of 5.625° (32×64 grid points) and 1.40625° (128×256 grid points). These weather variable maps capture global weather conditions, enabling the generation of forecast results.

3.2 Content Fusion Module

To improve and integrate the input data, we introduced the Content Fusion Module, which includes three key components: Detail-enhanced Convolution (DEConv), Spatial-Channel Attention (SCA), and Feature-guided Attention (FGA), as described in Figure 4. Additionally, the Features Fusion Processing is shown in Figure 3(b). These components work together to better integrate climatological mean state information during the forecasting process.

Detail-enhanced Convolution

While climatological mean state effectively captures overall weather trends, it fails to retain detailed variations at each moment [Kumar and Tiwari, 2023]. Previously, some researchers [Zhang and Patel, 2018; Wang *et al.*, 2021] have utilized edge priors to enhance details. Building on this work, we developed a Detail-enhanced Convolution (DEConv) layer (see Figure 4(left)) that extracts the climatological trend features at the forecast time. The formula is as follows:

$$C_{out} = DEConv(C_{t+n}) = C_{t+n} * (K + I) \quad (1)$$

where $DEConv(\cdot)$ denotes Detail-enhanced Convolution operation, K is the differential convolution kernels, $*$ denotes the convolution operation, and I is the identity matrix.

In differential convolution, pixel pair differences are calculated and prior information is explicitly encoded into the CNN, enhancing the model's representation by learning valuable trend information. Compared to complex enhancement algorithms, this method extracts richer features from climatological mean state by utilizing convolution layers.

Spatial-Channel Attention

The architecture of Spatial-Channel Attention (SCA) is designed to effectively model the intricate relationships present in weather data by addressing two key dimensions: spatial and channel dependencies. Spatial dependencies refer to how weather variables like temperature or pressure vary across regions, while channel dependencies focus on the relationships between different variables, such as how temperature and pressure interact. Together, these dependencies help the model understand atmospheric patterns and predict complex weather systems more accurately. The SCA primarily consists of Spatial Attention and Channel Attention, as illustrated in Figure 4 (middle). This structure provides two key benefits: (1) Spatial attention leverages spatial value-range variations (e.g., regional maxima and averages) to capture pixel-level features, denoted as F_s , and (2) Channel attention highlights feature-level differences across channels, represented

as F_c . Both F_s and F_c belong to $\mathbf{R}^{V \times H \times W}$. The features F_s and F_c are computed using the following formulas.

$$\begin{aligned} F_c &= \mathcal{C}_{1 \times 1}(\max(0, \mathcal{C}_{1 \times 1}(Y_{PAP}^c))), \\ F_s &= \mathcal{C}_{7 \times 7}([Y_{PAP}^s, Y_{PMP}^s]) \end{aligned} \quad (2)$$

where $\max(0, x)$ denotes the ReLU function, $\mathcal{C}_{k \times k}(\cdot)$ represents a convolution layer with a $k \times k$ kernel size, and $[\cdot]$ denotes channel-wise concatenation. Y_{PAP}^c , Y_{PAP}^s , and Y_{PMP}^s represent features processed by partial average pooling across the channel or spatial dimension and global max pooling across the spatial dimension, respectively.

Then we fuse F_c and F_s through element-wise addition to obtain the enhanced climate data $F_{add} \in \mathcal{R}^{V \times H \times W}$.

$$F_{add} = F_c + F_s \quad (3)$$

Note that the SCA generates feature information F_{add} for each variable, guiding the model to focus on important regions. It enables clearer and more refined results by adjusting each channel based on the corresponding input features.

Feature-guided Attention

We observed that fusing detail-enhanced features with spatial-channel information is an effective approach for improving long-term climate forecasting [Li *et al.*, 2024]. Research has shown that feature fusion can enhance these climate information features, aiding long-term predictions [Chen *et al.*, 2024]. However, mismatches may occur when fusing frequency features and trend information from input climate data. To address this, we propose Feature-guided Attention (FGA), as shown in Figure 4 (right), to guide the fusion process of the features F_{add} and C_{out} , ensuring a more accurate integration of climate features.

Figure 3 (b) illustrates the process of adaptively computing spatial weights from two input features for weighted fusion. The trend features produced by DEConv and the frequency features generated by SCA are passed into the FGA, which calculates the respective weights. These weights are then applied in a weighted summation to combine the features. Additionally, skip connections are incorporated to add input features, helping to mitigate the gradient vanishing problem. Finally, a 1×1 convolutional layer is applied to project the fused features, resulting in the final value of the input information.

$$\hat{y}_t = \mathcal{C}_{1 \times 1}(C_{out} \cdot W + F_{add} \cdot (\mathbf{1} - W) + C_{out} + F_{add}), \quad (4)$$

where $\mathbf{1}$ denotes a matrix with all elements equal to 1. W represents the calculated spatial weights. More comprehensive information integration is beneficial for learning in the subsequent PatchEmbedding layer.

3.3 Muti-layers PatchEmbedding

To capture interactions among variables at different pressure levels, the upper-air variables are structured as a (C, L, D) tensor, where C represents the number of pressure levels, L denotes the sequence length, and D indicates the embedding token length. Surface variables, which are influenced by terrain, land-sea mask, and soil conditions, are represented separately as an (L, D) tensor. The latent representations from each patch are merged into a $(C+1, L, D)$ tensor, serving

as the latent state for backbone input. To preserve latitude, longitude, and temporal information, these variables are first converted into D-dimensional tensors using Fourier encoding. The Fourier transform is implemented as follows:

$$\text{FourEnc}(x) = [\sin\left(\frac{2\pi x}{\lambda_i}\right), \cos\left(\frac{2\pi x}{\lambda_i}\right)], \quad (5)$$

$$\lambda_i = \lambda_{\min} \cdot \left(\frac{\lambda_{\max}}{\lambda_{\min}}\right)^{\frac{i-1}{(D/2)-1}}$$

where $i = 1, 2, \dots, D/2$, and λ_i represents the wavelength of the Fourier basis function, ensuring that the encoding captures various frequency components of the input variable. For time, since climate changes follow a yearly cycle, the wavelength range for time encoding can be set with $\lambda_{\min} = 1$ and $\lambda_{\max} = 365$. For position, the wavelength range can generally be set with $\lambda_{\min} = 0.1$ and $\lambda_{\max} = 360$, representing the spatial scale of longitude. After being processed by a linear layer, the temporal and spatial information are integrated into a $(C+1, D)$ tensor for fusion.

3.4 UD-ViT Backbone

Due to the accuracy demands of single-step predictions, the backbone neural network should exhibit some degree of generalization to systematic biases, thereby improving its ability to handle forecasts with different lead times.

Recent researches has explored how neural network architectures can integrate differential equations to achieve the desired effects [Michoski *et al.*, 2020; Yuan *et al.*, 2022]. Building on this, we observed that using a uncertainty block to fit partial differential equations (PDE), as the solution to the transport equation (TE), as shown in Eq.6, enhances generalization and accuracy [Yuan *et al.*, 2024].

$$\underbrace{\frac{\partial u}{\partial t}(\mathbf{x}, t) + F(\mathbf{x}, \theta(t)) \cdot \nabla u(\mathbf{x}, t)}_{\text{Transport Equation term}} + \underbrace{\frac{1}{2}G(\mathbf{x}, \phi(t))^2 \cdot \Delta u(\mathbf{x}, t)}_{\text{Uncertainty term}} = 0 \quad (6)$$

where $u(\mathbf{x}, t)$ represents the foundational function of the neural network. The variable $t \in (0, 1)$ denotes time. $\mathbf{x} \in \mathcal{R}^d$ represents the spatial variable used for data representation within the neural network. The gradient ∇u indicates gradient, and $F(\mathbf{x}, \theta(t))$ is the velocity field. $G(\mathbf{x}, \phi(t))^2$ is a coefficient function, exhibiting different uncertainty properties, based on the parameters ϕ at each time step t.

The content describes calculating $u(\mathbf{x}, t)$ by transporting the variable \mathbf{x} through $F(\mathbf{x}, \theta(t))$ over time, with the terminal condition enforced at $t = 1$. The method solves the original PDE using the method of characteristics, obtaining the solution by following the characteristic curves. Then the solution of PDE can be acquired by following these curves in Eq. 7.

$$u(\hat{\mathbf{x}}, 0) = \mathbb{E}[o(\mathbf{x}(1)) \mid \mathbf{x}(0) = \hat{\mathbf{x}}] \quad (7)$$

$$d\mathbf{x}(t) = F(\mathbf{x}(t), \theta(t))dt + G(\mathbf{x}(t), \phi(t)) \cdot dB_t$$

where dB_t represents the stochastic term. To solve Eq. 7 numerically, we adopt Euler method as shown in Eq. 8, which utilizes the structure of residuals [He *et al.*, 2016].

$$u(\hat{\mathbf{x}}, 0) = \mathbb{E}[o(f_L) \mid f_0 = \hat{\mathbf{x}}] \quad (8)$$

$$\tilde{f}_{l+1} = \tilde{f}_l + h(f_l, \theta_l) + g_l(f_l) \cdot \mathcal{N}(\mathbf{0}, \mathbf{I})$$

Type	Variable name	Abbrev.	Levels
Static	Land-sea mask	LSM	-
Static	Orography	-	-
Surface	2 metre temperature	T2m	-
Surface	10m Wind speed	Wind ₁₀	-
Upper	Geopotential	Z	50, 100, 150
Upper	Wind speed	Wind	200, 250, 300
Upper	Temperature	T	400, 500, 600
Upper	Specific humidity	Q	700, 850
Upper	Relative humidity	R	925, 1000

Table 1: Dataset Variable List for Different Types and Levels.

where $l \in \{1, \dots, L\}$ is the network layer index, serving as a discrete slicing to continuous time t . f_l and θ_l are representations and parameters at layer l , respectively. $o(h_L)$ the result after passing through L layers of Transformer blocks. $\tilde{f}_{l+1} = h(\tilde{f}_l, \theta_l)$ is the output of the l^{th} layer. $g_l(f_{l+1})$ is a learnable parameter generated by the uncertainty block.

Hence, we incorporated a uncertainty block into the original Vision Transformer (ViT) framework to align with the fluid dynamics in climate systems, as shown in Figure 3(c). The equation for the l^{th} layer as:

$$\tilde{f}_l = (g_{l-1} \circ (f_{l-1} + I) \circ \dots \circ g_1 \circ (f_1 + I))(\mathbf{x}) \quad (9)$$

For each block, the uncertainty block injects Gaussian noise, allowing the backbone network to learn data distributions at different lead times, thereby improving the presentation of finer details in predictions.

Unpatchify. The Module operation then reverses this process with an equal number of parameters, which are distinct from those used in Muti-layers PatchEmbedding.

3.5 Learning Objectives

Specifically, given the input current data y_t with a shape of $V \times H \times W$ at time t , TianQuan-Climate is trained to forecast the predictions $\tilde{y}_{t+\Delta t}$ with the same shape at lead time Δt . The objective function used is the latitude-weighted mean squared error [Rasp *et al.*, 2020]. The loss is calculated between the prediction $\tilde{y}_{t+\Delta t}$ and the ground truth $y_{t+\Delta t}$ as follows:

$$\mathcal{L} = \frac{1}{V \times H \times W} \sum_{v=1}^V \sum_{i=1}^H \sum_{j=1}^W L(i) \left(\tilde{y}_{t+\Delta t}^{v,i,j} - y_{t+\Delta t}^{v,i,j} \right)^2 \quad (10)$$

in which $L(i)$ is the latitude weighting factor:

$$L(i) = \frac{\cos(\text{lat}(i))}{\frac{1}{H} \sum_{i'=1}^H \cos(\text{lat}(i'))} \quad (11)$$

where $\text{lat}(i)$ represents the latitude of the i^{th} row in the grid. The difference in the coefficient size is due to the fact that grid cells near the equator cover more area than those near the poles, and are therefore assigned greater weight.

4 Experiments

4.1 Implementation Details

We used the AdamW optimizer [Kingma, 2014; Loshchilov and Hutter, 2017] with parameters $\lambda_1 = 0.9$ and $\lambda_2 = 0.99$. A

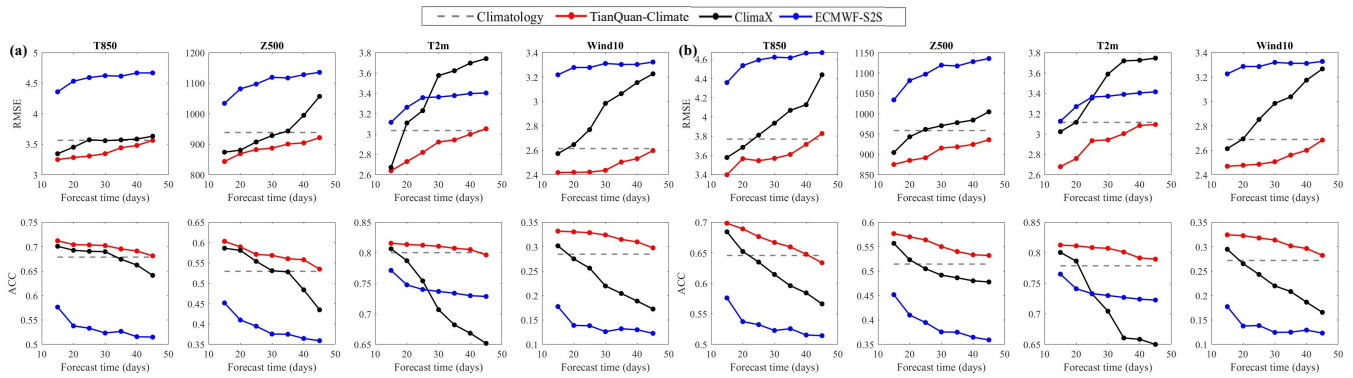


Figure 5: **TianQuan-Climate produces better performance than ClimaX and ECMWF-S2S in deterministic forecasts on 1.40625° (a) and 5.625° (b) daily ERA5 datasets.** The comparison involves four variables in terms of latitude-weighted RMSE (lower is better) and ACC (higher is better). The time range for the metric calculations is from 2017 to 2018.

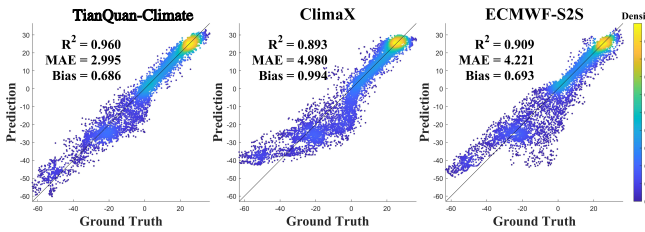


Figure 6: **Scatter chart of prediction and the ground true.** For 25-day predictions of T2m, the closer the scatter points are to the diagonal line, the smaller the error in this case. The input time is 00:00 UTC on 15 February 2017.

weight decay of 1×10^{-5} was applied to all parameters except the positional embeddings. The learning rate was set to 5×10^{-5} , with a linear warmup schedule over 5000 steps (5 epochs), followed by a cosine annealing schedule over 95000 steps (95 epochs). Our model training were implemented using PyTorch [Paszke *et al.*, 2019].

In the training process, We train multiple models with different lead time settings, where the lead time ranges from 15 to 45 days with an interval of 5 days. The output from each model, corresponding to a single step prediction, is combined to form a 45-day subseasonal forecast target. The model was trained on eight GPUs with 80GB memory, achieving 77.6 TFLOPS of computing power.

4.2 Experiment Settings

Datasets. We conducted experiments using the ERA5 dataset [Hersbach *et al.*, 2018] from the European Centre for Medium-Range Weather Forecasts (ECMWF). The dataset spans 40 years, from 1979 to 2018, on a global $0.25^\circ \times 0.25^\circ$ latitude-longitude grid, with hourly data recorded at 37 different pressure levels and the surface, comprising a total of 721×1440 grid points. In order to enhance the accuracy and effectiveness of long-term predictions, we use daily averages to pretreat the hourly ERA5 data at six-hour intervals, while downsampling was performed using bilinear interpolation to 5.625° (32×64 grid points) and 1.40625° (128×256 grid points) and selecting the 13 most critical levels. Hence, we

Model	Vars	15 days			35 days		
		CRPS \downarrow	SME \downarrow	RQE \downarrow	CRPS \downarrow	SME \downarrow	RQE \downarrow
ClimaX	T850	2.821	2.33	2.748	2.839	2.404	2.950
	Z500	650.0	654.8	653.4	658.4	666.5	777.0
	T2m	2.278	2.19	2.187	2.475	2.433	2.562
	Wind ₁₀	1.801	1.05	1.747	1.811	1.058	1.848
Ours	T850	2.805	2.301	2.711	2.826	2.378	2.753
	Z500	644.3	649.9	620.3	653.1	656.2	674.2
	T2m	2.256	2.048	2.158	2.318	2.328	2.417
	Wind ₁₀	1.799	1.04	1.729	1.804	1.052	1.804

Table 2: Performance Metrics for Different Models and Variables

obtained the dataset variables as shown in Table 1.

Metrics. We primarily quantify the performance improvement of the model using ACC and RMSE, and then assess its long-term forecasting capability through CRPS, SME, and RQE. These metrics have been applied in climate forecasting [Bi *et al.*, 2023].

Baselines. At the same resolution, We compare our proposed model with the following baseline models:

- **ECMWF-S2S** [Vitart *et al.*, 2017] is a WWRP/THOR PEX-WCRP joint research project established to improve forecast skill and understanding on the subseasonal to seasonal time scale.
- **ClimaX** [Nguyen *et al.*, 2023] is a deep learning foundational model for weather and climate science, capable of training on heterogeneous datasets with varying variables and spatio-temporal coverage.
- **Climatology** utilizes the long-term average of historical data for each time step as the reference prediction, providing a simple yet effective benchmark for comparison.

4.3 Main Results

The experimental results primarily highlight two key advantages of the proposed model. First, it mitigates the blurring effects commonly observed in machine learning models during subseasonal forecasts, enhancing feature details. Second, it reduces the errors accumulation over extended time scales, improving various climate evaluation metrics, such as RMSE, ACC, and CRPS.

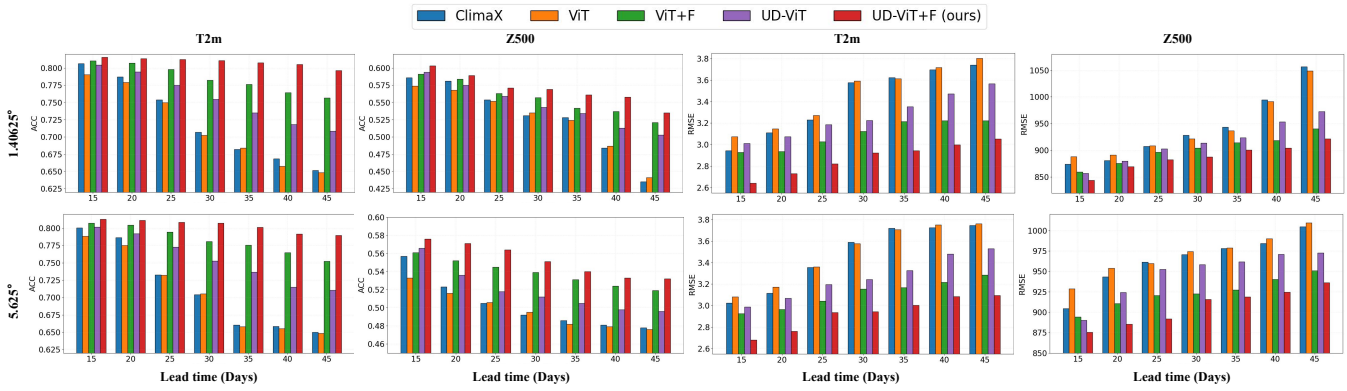


Figure 7: **Comparison of Ablation Experiments for Four Experimental Models and ClimaX.** The metrics for 15-45 day lead time predictions of Z500 and T2m variables on data with 1.40625° and 5.625° resolutions. The 'F' denotes the Content Fusion Module.

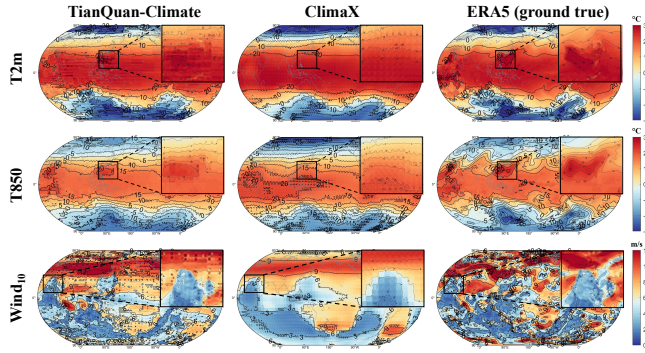


Figure 8: **Visualization of forecast results on 1.40625° daily ERA5 data.** The 30-day forecast of one upper-air variable (T850) and two surface variables (T2m and Wind₁₀). For each case, the top right corner shows an enlarged comparison of the local area details. For all cases, the input time is 00:00 UTC on 15 February 2018.

Quantitative Comparison. We compare the ACC and RMSE of TianQuan-Climate for lead times of 15-45 days with the baselines in Figure 5. Regardless of whether the resolution is 1.40625° or 5.625° , for each test variable, including both upper-atmosphere and surface variables, TianQuan-Climate demonstrated higher accuracy than ECMWF-S2S and ClimaX. This advantage was consistent across all lead times and became more pronounced as the forecast period extended. In terms of RMSE (lower is better), TianQuan-Climate reported values that were on average 21% lower than ECMWF-S2S and 10% lower than ClimaX. Note that, before the 45-day forecast metric, our model shows an improvement in metrics compared to Climatology. Figure 6 shows the scatter plot distribution for 25-day predictions of the T2m variable. Our method is closer to the true values, and outperforms ECMWF-S2S and ClimaX across correlation (R^2), mean average error (MAE), and Bias metrics. This signifies a substantial reduction in cumulative errors for long-term forecasts.

Metric Function Effectiveness. Table 2 compares the performance of TianQuan-Climate and ClimaX in terms of long-term forecast metrics. In these metrics, our model shows performance improvement compared to ClimaX. It demonstrates

that the designed functional modules are effective.

Detailed Visualization. Figure 8 illustrates the performance of the proposed model compared to the baseline (ClimaX) in predicting three target variables (T2m, T850, and Wind₁₀). Overall, our proposed model captures more details across the three variables, similar to the ERA5 data. Particularly in regions with significant variations, the proposed model more accurately reflects the temperature fluctuations observed in the ERA5 data. In summary, our proposed model effectively addresses the unrealistic blurring issues commonly seen in subseasonal forecasting with machine learning models.

4.4 Ablation Study

We conducted ablation studies to compare four experimental models and ClimaX, analyzing the impact of different components on forecast performance as shown in Figure 7.

Fusion Climatology Gain. Comparing the models with and without the 'F' module, it is evident that incorporating climatology information significantly improves the metrics for forecasts beyond 25 days, indicating that the trend information provided by the climatology is crucial. However, as observed in Figure 5, the ACC and RMSE metrics for the 45-day forecast show that for both resolution, some variables in the model with fusion perform worse than Climatology. This suggests that the performance gains from the information fusion gradually diminish after 45 days.

Backbone Adaptability. The model with UD-ViT as the backbone, as shown in Figure 7, demonstrates a noticeable improvement in performance across various lead times compared to the original ViT model. Note that, there is also an improvement after incorporating climatology information into the original model.

Base Backbone Selection. Comparing ClimaX and ViT, we observe little performance difference in the 15-45 day predictions, suggesting that ClimaX's performance has degraded to a level similar to that of the ViT model for long-term forecasts. Therefore, considering training costs, our model is modified based on ViT backbone.

5 Conclusion

In this paper, we introduce TianQuan-Climate, a machine learning model that supports SDGs, including sustainable energy and climate change challenge by providing global daily mean climate forecasts up to 45 days. To tackle cumulative system errors in long-term forecasts, we employ a multi-model single-step prediction approach, which reduces numbers of error accumulation. We proposed the Content Fusion Module and extend the Vision Transformer with uncertainty blocks (UD-ViT) to improve the model's single-step prediction accuracy across varying lead times. Experimental results show that TianQuan-Climate outperforms existing traditional models and AI methods in the 15–45 days subseasonal forecast range.

References

[Bauer *et al.*, 2015] Peter Bauer, Alan Thorpe, and Gilbert Brunet. The quiet revolution of numerical weather prediction. *Nature*, 525(7567):47–55, 2015.

[Bauer *et al.*, 2020] Peter Bauer, Tiago Quintino, Nils Wedi, Antonio Bonanni, Marcin Chrst, Willem Deconinck, Michail Diamantakis, Peter Düben, Stephen English, Johannes Flemming, et al. The ECMWF scalability programme: Progress and plans. European Centre for Medium Range Weather Forecasts, 2020.

[Beljaars *et al.*, 2018] Anton Beljaars, Gianpaolo Balsamo, Peter Bechtold, Alessio Bozzo, Richard Forbes, Robin J Hogan, Martin Köhler, Jean-Jacques Morcrette, Adrian M Tompkins, Pedro Viterbo, et al. The numerics of physical parametrization in the ecmwf model. *Frontiers in Earth Science*, 6:137, 2018.

[Bi *et al.*, 2023] Kaifeng Bi, Lingxi Xie, Hengheng Zhang, Xin Chen, Xiaotao Gu, and Qi Tian. Accurate medium-range global weather forecasting with 3d neural networks. *Nature*, 619(7970):533–538, 2023.

[Bonavita, 2023] Massimo Bonavita. On the limitations of data-driven weather forecasting models. *arXiv preprint arXiv:2309.08473*, 2023.

[Chen *et al.*, 2023] Lei Chen, Xiaohui Zhong, Feng Zhang, Yuan Cheng, Yinghui Xu, Yuan Qi, and Hao Li. Fuxi: A cascade machine learning forecasting system for 15-day global weather forecast. *npj Climate and Atmospheric Science*, 6(1):190, 2023.

[Chen *et al.*, 2024] Lei Chen, Xiaohui Zhong, Hao Li, Jie Wu, Bo Lu, Deliang Chen, Shang-Ping Xie, Libo Wu, Qingchen Chao, Chensen Lin, et al. A machine learning model that outperforms conventional global subseasonal forecast models. *Nature Communications*, 15(1):6425, 2024.

[Cohen *et al.*, 2019] Judah Cohen, Dim Coumou, Jessica Hwang, Lester Mackey, Paulo Orenstein, Sonja Totz, and Eli Tziperman. S2s reboot: An argument for greater inclusion of machine learning in subseasonal to seasonal forecasts. *Wiley Interdisciplinary Reviews: Climate Change*, 10(2):e00567, 2019.

[He *et al.*, 2016] Kaiming He, Xiangyu Zhang, Shaoqing Ren, and Jian Sun. Deep residual learning for image recognition. *IEEE*, 2016.

[He *et al.*, 2019] Zheng He, Pangchi Hsu, Xiangwen Liu, Tongwen Wu, and Yingxia Gao. Factors limiting the forecast skill of the boreal summer intraseasonal oscillation in a subseasonal-to-seasonal model. *Advances in Atmospheric Sciences*, 36:104–118, 2019.

[He *et al.*, 2021] Sijie He, Xinyan Li, Timothy DelSole, Pradeep Ravikumar, and Arindam Banerjee. Sub-seasonal climate forecasting via machine learning: Challenges, analysis, and advances. In *Proceedings of the AAAI Conference on Artificial Intelligence*, volume 35, pages 169–177, 2021.

[Hersbach *et al.*, 2018] Hans Hersbach, Bill Bell, Paul Berrisford, Gionata Biavati, András Horányi, Joaquín Muñoz Sabater, Julien Nicolas, Carole Peubey, Raluca Radu, Iryna Rozum, et al. Era5 hourly data on single levels from 1979 to present. *Copernicus climate change service (c3s) climate data store (cds)*, 10(10.24381), 2018.

[Kingma, 2014] DP Kingma. Adam: a method for stochastic optimization. *arXiv preprint arXiv:1412.6980*, 2014.

[Kochkov *et al.*, 2024] Dmitrii Kochkov, Janni Yuval, Ian Langmore, Peter Norgaard, Jamie Smith, Griffin Mooers, Milan Klöwer, James Lottes, Stephan Rasp, Peter Düben, et al. Neural general circulation models for weather and climate. *Nature*, pages 1–7, 2024.

[Kumar and Tiwari, 2023] Harshvardhan Kumar and Shani Tiwari. Climatology, trend of aerosol-cloud parameters and their correlation over the northern indian ocean. *Geoscience Frontiers*, 14(4):101563, 2023.

[Lam *et al.*, 2022] Remi Lam, Alvaro Sanchez-Gonzalez, Matthew Willson, Peter Wirnsberger, Meire Fortunato, Ferran Alet, Suman Ravuri, Timo Ewalds, Zach Eaton-Rosen, Weihua Hu, et al. Graphcast: Learning skillful medium-range global weather forecasting. *arXiv preprint arXiv:2212.12794*, 2022.

[Lam *et al.*, 2023] Remi Lam, Alvaro Sanchez-Gonzalez, Matthew Willson, Peter Wirnsberger, Meire Fortunato, Ferran Alet, Suman Ravuri, Timo Ewalds, Zach Eaton-Rosen, Weihua Hu, et al. Learning skillful medium-range global weather forecasting. *Science*, 382(6677):1416–1421, 2023.

[Li *et al.*, 2024] Haipeng Li, Kunming Luo, Bing Zeng, and Shuaicheng Liu. Gyroflow+: Gyroscope-guided unsupervised deep homography and optical flow learning. *International Journal of Computer Vision*, 132(6):2331–2349, 2024.

[Loshchilov and Hutter, 2017] Ilya Loshchilov and Frank Hutter. Decoupled weight decay regularization. *arXiv preprint arXiv:1711.05101*, 2017.

[Mariotti *et al.*, 2018] Annarita Mariotti, Paolo M Ruti, and Michel Rixen. Progress in subseasonal to seasonal prediction through a joint weather and climate community effort. *Npj Climate and Atmospheric Science*, 1(1):4, 2018.

[Michoski *et al.*, 2020] Craig Michoski, Miloš Milosavljević, Todd Oliver, and David R Hatch. Solving differential equations using deep neural networks. *Neurocomputing*, 399:193–212, 2020.

[Nathaniel *et al.*, 2024] Juan Nathaniel, Yongquan Qu, Tung Nguyen, Sungduk Yu, Julius Busecke, Aditya Grover, and Pierre Gentine. Chaosbench: A multi-channel, physics-based benchmark for subseasonal-to-seasonal climate prediction. *arXiv preprint arXiv:2402.00712*, 2024.

[Nguyen *et al.*, 2023] Tung Nguyen, Johannes Brandstetter, Ashish Kapoor, Jayesh K Gupta, and Aditya Grover. Climax: A foundation model for weather and climate. *arXiv preprint arXiv:2301.10343*, 2023.

[of Sciences *et al.*, 2016] National Academies of Sciences, Division on Earth, Life Studies, Ocean Studies Board, Board on Atmospheric Sciences, and Committee on Developing a US Research Agenda to Advance Subseasonal to Seasonal Forecasting. *Next generation earth system prediction: strategies for subseasonal to seasonal forecasts*. National Academies Press, 2016.

[Paszke *et al.*, 2019] Adam Paszke, Sam Gross, Francisco Massa, Adam Lerer, James Bradbury, Gregory Chanan, Trevor Killeen, Zeming Lin, Natalia Gimelshein, Luca Antiga, et al. Pytorch: An imperative style, high-performance deep learning library. *Advances in neural information processing systems*, 32, 2019.

[Pathak *et al.*, 2022] Jaideep Pathak, Shashank Subramanian, Peter Harrington, Sanjeev Raja, Ashesh Chattopadhyay, Morteza Mardani, Thorsten Kurth, David Hall, Zongyi Li, Kamyar Azizzadenesheli, et al. Fourcastnet: A global data-driven high-resolution weather model using adaptive fourier neural operators. *arXiv preprint arXiv:2202.11214*, 2022.

[Pegion *et al.*, 2019] Kathy Pegion, Ben P Kirtman, Emily Becker, Dan C Collins, Emerson LaJoie, Robert Burgman, Ray Bell, Timothy DelSole, Dughong Min, Yuejian Zhu, et al. The subseasonal experiment (subx): A multimodel subseasonal prediction experiment. *Bulletin of the American Meteorological Society*, 100(10):2043–2060, 2019.

[Price *et al.*, 2024] Ilan Price, Alvaro Sanchez-Gonzalez, Ferran Alet, Tom R Andersson, Andrew El-Kadi, Dominic Masters, Timo Ewalds, Jacklynn Stott, Shakir Mohamed, Peter Battaglia, et al. Probabilistic weather forecasting with machine learning. *Nature*, 637(8044):84, 2024.

[Rasp *et al.*, 2020] Stephan Rasp, Peter D Dueben, Sebastian Scher, Jonathan A Weyn, Soukaina Mouatadid, and Nils Thuerey. Weatherbench: a benchmark data set for data-driven weather forecasting. *Journal of Advances in Modeling Earth Systems*, 12(11):e2020MS002203, 2020.

[Robertson *et al.*, 2020] Andrew W Robertson, Frederic Vitart, and Suzana J Camargo. Subseasonal to seasonal prediction of weather to climate with application to tropical cyclones. *Journal of Geophysical Research: Atmospheres*, 125(6):e2018JD029375, 2020.

[Saha *et al.*, 2014] Suranjana Saha, Shrinivas Moorthi, Xingren Wu, Jiande Wang, Sudhir Nadiga, Patrick Tripp, David Behringer, Yu-Tai Hou, Hui-ya Chuang, Mark Iredell, et al. The ncep climate forecast system version 2. *Journal of climate*, 27(6):2185–2208, 2014.

[Vitart *et al.*, 2017] Frederic Vitart, Constantin Ardilouze, Axel Bonet, Anca Brookshaw, M Chen, C Codorean, M Déqué, L Ferranti, E Fucile, M Fuentes, et al. The subseasonal to seasonal (s2s) prediction project database. *Bulletin of the American Meteorological Society*, 98(1):163–173, 2017.

[Vitart *et al.*, 2019] Frédéric Vitart, Christopher Cunningham, Michael DeFlorio, Emanuel Dutra, Laura Ferranti, Brian Golding, Debra Hudson, Charles Jones, Christophe Lavaysse, Joanne Robbins, et al. Sub-seasonal to seasonal prediction of weather extremes. In *Sub-seasonal to seasonal prediction*, pages 365–386. Elsevier, 2019.

[Vitart *et al.*, 2022] Frederic Vitart, Andrew W Robertson, Aaron Spring, Florian Pinault, Rok Roškar, W Cao, S Bech, A Bienkowski, N Caltabiano, E De Coning, et al. Outcomes of the wmo prize challenge to improve subseasonal to seasonal predictions using artificial intelligence. *Bulletin of the American Meteorological Society*, 103(12):E2878–E2886, 2022.

[Wang *et al.*, 2021] Chao Wang, Hao-Zhen Shen, Fan Fan, Ming-Wen Shao, Chuan-Sheng Yang, Jian-Cheng Luo, and Liang-Jian Deng. Eaa-net: A novel edge assisted attention network for single image dehazing. *Knowledge-Based Systems*, 228:107279, 2021.

[Wang *et al.*, 2024] Chenggong Wang, Michael S Pritchard, Noah Brenowitz, Yair Cohen, Boris Bonev, Thorsten Kurth, Dale Durran, and Jaideep Pathak. Coupled ocean-atmosphere dynamics in a machine learning earth system model. *arXiv preprint arXiv:2406.08632*, 2024.

[Yuan *et al.*, 2022] Lei Yuan, Yi-Qing Ni, Xiang-Yun Deng, and Shuo Hao. A-pinn: Auxiliary physics informed neural networks for forward and inverse problems of nonlinear integro-differential equations. *Journal of Computational Physics*, 462:111260, 2022.

[Yuan *et al.*, 2024] Yige Yuan, Bingbing Xu, Bo Lin, Liang Hou, Fei Sun, Huawei Shen, and Xueqi Cheng. Pde+: Enhancing generalization via pde with adaptive distributional diffusion. In *Proceedings of the AAAI Conference on Artificial Intelligence*, volume 38, pages 16614–16622, 2024.

[Zhang and Patel, 2018] He Zhang and Vishal M Patel. Densely connected pyramid dehazing network. In *Proceedings of the IEEE conference on computer vision and pattern recognition*, pages 3194–3203, 2018.

Appendix

A Model Details

This section presents the improved detailsof TianQuan-Climate.

Improved details

After comparing our proposed TianQuan-Climate with ClimaX in the experiments, we identified the following details as critical for subseasonal forecasts performance:

- **Multi-scale Temporal Modeling:** Capturing features at different time scales is crucial for subseasonal forecasts. Using multi-scale convolutions or multi-layer recurrent neural networks can effectively handle both short-term and long-term dependencies.
- **Incorporation of Attention Mechanisms:** Self-attention mechanisms can dynamically assign importance to different time steps, allowing the model to focus more on the time steps that have a greater impact on future predictions, thereby improving accuracy.
- **Residual and Skip Connections:** Adding residual or skip connections in deep neural networks can alleviate the vanishing gradient problem, enhancing the model’s ability to capture long-term dependencies.
- **Climate change trend information:** For time series with significant seasonality and long-term climate trends, enhancing and fusing climate features separately can significantly improve prediction performance.

Hyperparameters

The hyperparameters of the model are shown in Table 3.

Hyperparam	Meaning	Value
$ \mathcal{V} $	Number of default variables	67
D	Embedding dimension	384
Depth	Number of UD-ViT blocks	8
heads	Number of attention heads	12
Drop path	For stochastic depth	0.1
Dropout	Dropout rate	0.12

Table 3: Hyperparameters and their meanings for the model.

B Employed Data

In this paper, two pre-generated datasets, ERA5 and ECMWF-S2S, are primarily utilized. The following sections will introduce their sources and respective roles.

ERA5

We used the ERA5 [Rasp *et al.*, 2020] dataset to complete the model training process. ERA5 was created as a standard benchmark dataset and evaluation framework for comparing data-driven weather forecasting models. WeatherBench regridded the original ERA5 from 0.25° to three lower resolutions: 5.625° and 1.40625° . The corresponding data can be downloaded from <https://cds.climate.copernicus.eu/cdsapp#!/dataset/reanalysis-era5-complete?tab=overview>.

ECMWF-S2S

The Sub-seasonal to Seasonal Prediction Project (S2S) [Vitart *et al.*, 2017], initiated in November 2013 by the World Weather Research Programme (WWRP) and the World Climate Research Programme (WCRP), aims to enhance forecast skill and deepen our understanding of the dynamics and climate drivers on the sub-seasonal to seasonal timescale (ranging from two weeks to a season). This project seeks to bridge the gap between medium-range and seasonal forecasting by leveraging the combined expertise of the weather and climate research communities, thereby addressing critical issues relevant to the Global Framework for Climate Services (GFCS). We can download its data from <https://apps.ecmwf.int/datasets/data/s2s/>

C Quantitative evaluation

Metrics

In this section, we detail the evaluation metrics applied in our experiments. The predictions and ground truth are formatted as $N \times H \times W$, where N indicates the quantity of predictions or test samples, and $H \times W$ defines the spatial resolution. To address the varying sizes of grid cells, $\bar{L}(i)$ is introduced as a latitude-based weighting factor.

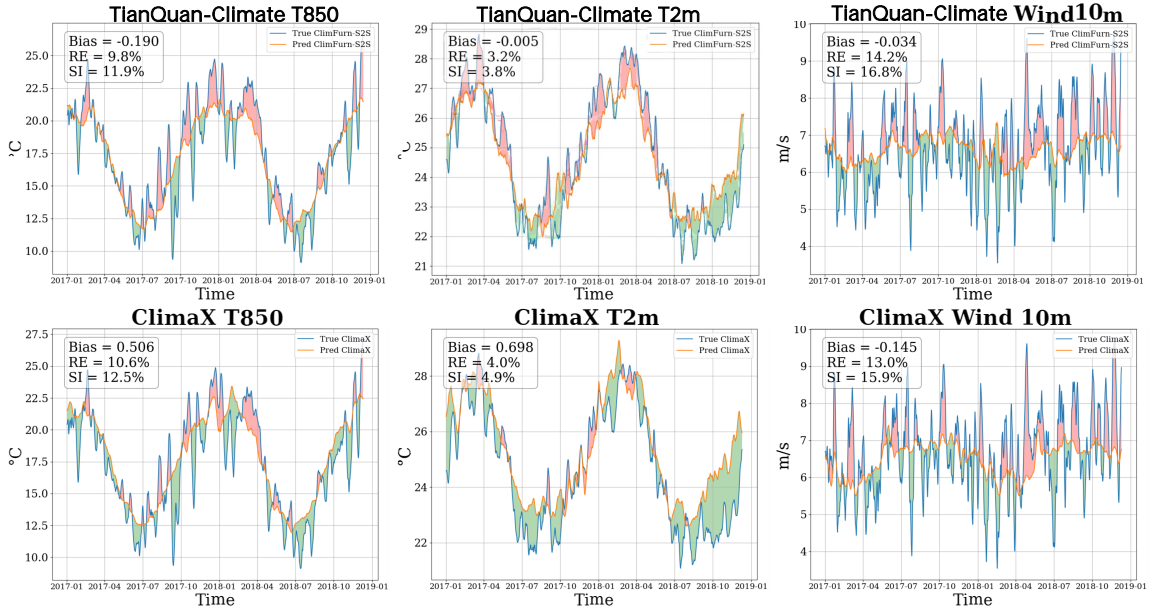


Figure 9: **Fixed-point time series diagrams for TianQuan-Climate and ClimaX across three variables (T850, T2m, and Wind₁₀).** The time series covers the period from 2017 to 2018, with latitude and longitude fixed at 23° and 113°.

Root mean square error (RMSE)

Root mean square error (RMSE) measures the average magnitude of the prediction errors in a dataset. It quantifies how closely predicted values match the actual values, with lower RMSE indicating more accurate predictions.

$$\text{RMSE} = \frac{1}{N} \sum_{k=1}^N \sqrt{\frac{1}{H \times W} \sum_{i=1}^H \sum_{j=1}^W L(i)(\tilde{y}_{k,i,j} - y_{k,i,j})^2} \quad (12)$$

Anomaly correlation coefficient (ACC)

Anomaly Correlation Coefficient (ACC) assesses the accuracy of a forecast by measuring the correlation between predicted and observed anomalies. It is commonly used in climate and weather forecasting to evaluate how well the model captures deviations from the climatological average. Higher ACC values indicate better predictive skill.

$$\text{ACC} = \frac{\sum_{k,i,j} L(i) \tilde{Y}'_{k,i,j} Y'_{k,i,j}}{\sqrt{\sum_{k,i,j} L(i) \tilde{Y}'_{k,i,j}^2 \sum_{k,i,j} L(i) Y'_{k,i,j}^2}} \quad (13)$$

$$\tilde{Y}'_{k,i,j} = \tilde{y}'_{k,i,j} - C_{k,i,j}, \quad y'_{k,i,j} = y'_{k,i,j} - C_{k,i,j} \quad (14)$$

where Climatology C represents the average of the ground truth data across the entire test set over time.

R-squared (R²), Mean Absolute Error (MAE) and Bias

R-squared (R²), Mean Absolute Error (MAE) and Bias are commonly used to assess the performance of predictive models. The metrics are shown in Figure 6.

$$R^2 = 1 - \frac{\sum_{i=1}^N (y_i - \hat{y}_i)^2}{\sum_{i=1}^N (y_i - \bar{y})^2} \quad (15)$$

$$MAE = \frac{1}{N} \sum_{i=1}^N |y_i - \hat{y}_i| \quad (16)$$

$$Bias = \frac{1}{N} \sum_{i=1}^N (\hat{y}_i - y_i) \quad (17)$$

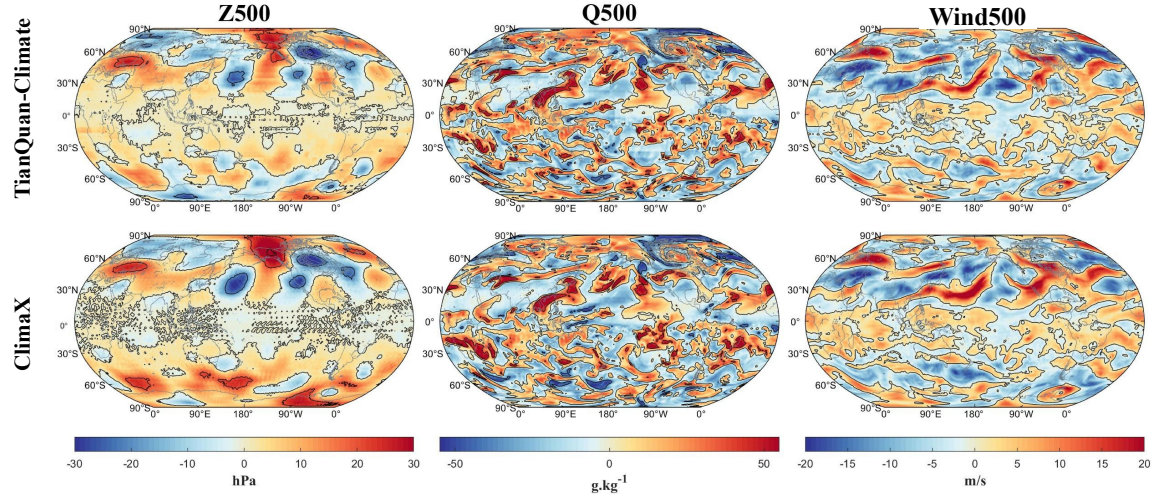


Figure 10: **Comparison of TianQuan-Climate and ClimaX in predicting deviations for three atmospheric variables: Z500, Q500, and Wind500.** The top row shows deviations from TianQuan-Climate, and the bottom row from ClimaX.

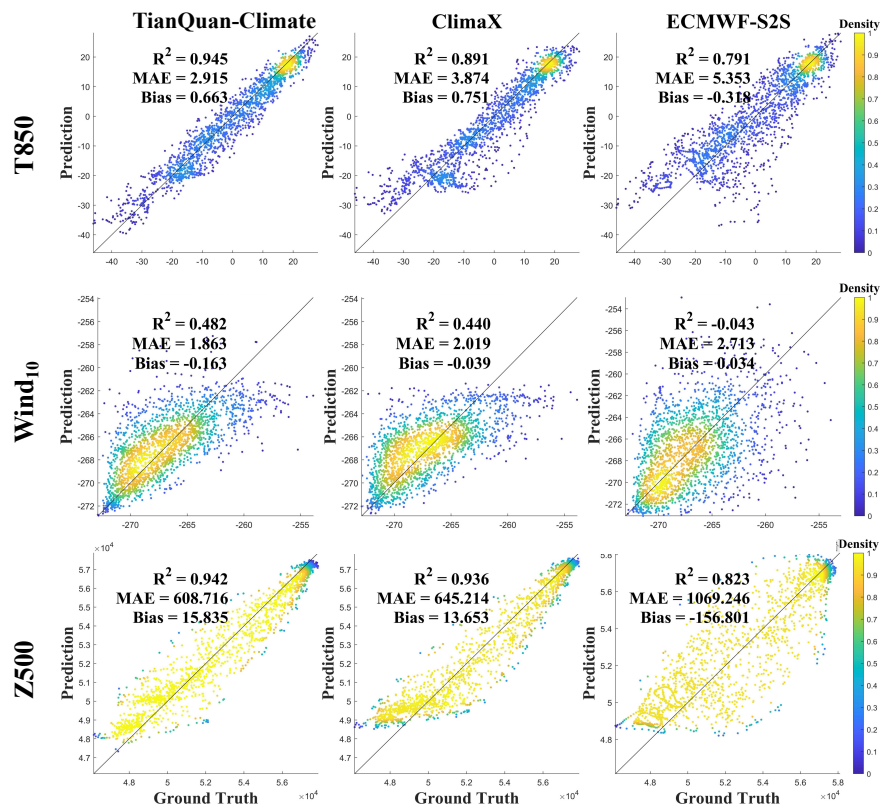


Figure 11: **The scatter plots in the figure compare the performance of TianQuan-Climate, ClimaX, and ECMWF-S2S across three variables: T850, Wind10, and Z500.** Each model's predictions are plotted against the ground truth, with density colors indicating the concentration of data points. The performance metrics, including R^2 , MAE, and Bias, are provided for each model.

Relative Error (RE) and Skill Index (SI)

Relative Error (RE) and Skill Index (SI) provide a way to assess the accuracy and skill of the forecasting models based on their deviations from actual observed data.

$$RE = \frac{|\hat{y} - y|}{|y|} \times 100\% \quad (18)$$

$$SI = \frac{RMSE}{\sigma_{obs}} \quad (19)$$

where σ_{obs} is the standard deviation of the observed values.

Continuous Ranked Probability Score (CRPS)

CRPS measures the difference between the forecast CDF and the step function at the observed value, thus evaluating both the sharpness and reliability of a probabilistic forecast. A lower CRPS indicates a more accurate forecast. **Calculation Formula:**

$$CRPS(F, y) = \int_{-\infty}^{+\infty} \left(F(x) - \mathbf{1}\{x \geq y\} \right)^2 dx, \quad (20)$$

where $F(x)$ is the forecast cumulative distribution function (CDF) and $\mathbf{1}\{x \geq y\}$ is the indicator function for the observed value y .

Spread Mean Error (SME)

SME quantifies the difference between the ensemble spread and the absolute error of the ensemble mean. This metric is useful to determine whether the ensemble is under-dispersive (negative SME) or over-dispersive (positive SME), and thus helps in assessing the reliability of the ensemble prediction system. **Calculation Formula:**

$$SME = \frac{1}{N} \sum_{i=1}^N (\sigma_i - |y_i - \mu_i|), \quad (21)$$

where for each case i , σ_i is the ensemble spread (e.g., the standard deviation), μ_i is the ensemble mean, and y_i is the observed value.

Relative Quantile Error (RQE)

RQE measures the relative error between the forecast quantiles and the observation across different probability levels. It helps to assess how well the forecast distribution captures the observed outcome. A lower RQE indicates that the forecast quantiles are in closer agreement with the observations, implying a more skillful probabilistic forecast. **Calculation Formula:**

Assuming K quantile levels α_k , RQE is defined as:

$$RQE = \frac{1}{K} \sum_{k=1}^K w_k \left| \frac{q_{\alpha_k} - y}{y} \right|, \quad (22)$$

where q_{α_k} denotes the forecast quantile at probability level α_k , y is the observed value, and w_k are the weights (with $\sum_{k=1}^K w_k = 1$).

D Additional Results

Figure 9 primarily illustrates the differences between pointwise time series predictions and actual values on 5.625° data. The results show that both TianQuan-Climate and ClimaX, as machine learning methods, can effectively capture the temperature trends associated with seasonal changes, demonstrating the advantages of machine learning in climate forecasting. Although there is still some deviation in more complex variables like 10m wind speed, both methods achieve relatively stable forecasting. Notably, TianQuan-Climate outperforms ClimaX in long-term sequence metrics such as RE and SI on the variable of temperature, but ClimaX is better on the variable of wind.

The Figure 10 illustrates the deviation of predictions from actual values for Z500, Q500, and W500 variables using TianQuan-Climate and ClimaX. Overall, TianQuan-Climate exhibits more accurate predictions with smaller and more evenly distributed deviations across all three variables, indicating better alignment with the actual atmospheric patterns. In contrast, ClimaX shows larger deviations, particularly in areas with more complex dynamics, suggesting it struggles to capture finer details and variations. The results demonstrate TianQuan-Climate's superior capability in minimizing prediction errors across different atmospheric conditions.

The results shown in Figure 11 indicate the following: For the Wind10 and Z500 variables, all models show a reduction in predictive accuracy compared to T850, with lower R^2 values across the board. Despite this, TianQuan-Climate consistently outperforms the other models. It achieves the highest R^2 values for both Wind10 (0.482) and Z500 (0.942), along with the lowest MAE values (1.863 and 608.716, respectively), indicating superior precision. While ClimaX performs reasonably well, its accuracy is slightly diminished, as reflected in its higher MAE and marginally lower R^2 values. ECMWF-S2S, however, struggles significantly with both variables, displaying minimal correlation with the ground truth, especially in Wind10, where it shows almost no predictive capability. The results confirm TianQuan-Climate's robustness across varying atmospheric conditions, while ClimaX and ECMWF-S2S show limitations in handling more complex variables like Wind10 and Z500.